

Evaluation of shear carried by steel fibers in reinforced concrete beams with steel fibers

K. Watanabe, P. Jongvivatsakul, & J. Niwa
 Tokyo Institute of Technology, Tokyo, Japan

T. Kimura
 Taisei Corporation, Tokyo, Japan

ABSTRACT: Reinforced concrete with steel fiber (RSF) beam is superior to ordinary RC beams in shear strength and ductility because of high energy absorption at fracture. On the other hand, the shear strength of RSF beams with stirrups has not been clarified yet. The objective of this study is to explain the shear strength of RSF beams with stirrups. The tension softening diagram, which is one of the fracture parameters, seems to be effective to explain the shear resistance mechanism of RSF beams as well as the increment of shear by mixing steel fibers in concrete. The crack width of the diagonal crack has been measured through the image analysis, and the shear carried by steel fiber was calculated based on the tension softening curve.

1 INTRODUCTION

The standard specifications of civil engineering structures have required providing large amount of steel bars to prevent shear failure. It leads to make difficult to fill up concrete during a construction. One of the methods to overcome this problem is the application of short fiber. Many researchers have reported that the addition of steel fibers can significantly increase the shear strength and ductility of reinforced concrete (RC) members, because the bridging effect of steel fibers will prevent the propagation of cracks. Japanese design guidelines for reinforced concrete piers with steel fiber (RSF) (JSCE 1999) have regarded steel fibers as the reinforcement for the shear failure of concrete. The prediction equation for the shear strength of RSF piers proposed in the design guidelines has been recommended to use for steel fibers with volume fraction of between 1.0 to 1.5 % of concrete full volume. One of the reasons for the limitation is that some previous studies on RSF piers have discussed the shear carried by steel fibers of the RC members without stirrups.

JSCE guidelines (1999) concluded that the increment of shear strength by fiber was expressed as a ratio of shear carried by concrete, V_c . The ratio, κ_{exp} , has been considered 1.0. Watanabe et al. (2008) stated that the value of κ_{exp} was, however, varied by the volume fraction of steel fibers (SF) and the stirrup ratio (r_w) of RSF beams. The arrangement of stirrups was effective to increase the shear carried by steel fibers as well as to reduce the variation of κ_{exp} . A combination of steel fibers and stirrups had a syner-

getic effect to increase the shear strength of concrete beams. In addition, there was an optimized combination of SF and r_w to increase the value of κ_{exp} . Authors stated that the optimized combination would be related to the length and crack width of the diagonal crack in Watanabe et al. (2008).

The target of this study is to make clear the synergetic effect of stirrups and steel fibers to a shear resistance of RSF beams. This study focused on the tension softening curve to evaluate the tensile stress transferring the diagonal crack. A series of bending tests of RSF beams with different stirrup ratio was conducted, and the effect of both reinforcements on the shear strength of RSF beams was examined. We considered the shear force transferred by the bridging effect of steel fibers, which worked as a function of the length and crack width of the diagonal crack. The force transferring across the diagonal crack would be increased with the increase in the diagonal crack length, and be decreased with the increase in the diagonal crack width. The force was evaluated associated with the tension softening curve. Finally, this study explained the shear carried by steel fibers.

Table 1. Mix proportions of concrete.

G_{max}^{*1} (mm)	Slump (cm)	W/C	Unit weight (kg/m ³)				SP ^{*2}
			Water	Cement	Sand	Gravel	
20	17	0.35	165	471	917	790	5.2

*1: Maximum size of aggregate, *2: Superplasticizer.

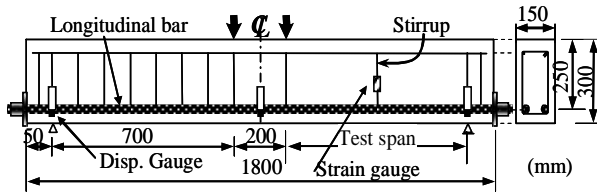


Figure 1. Outline of tested RSF beam.

2 EXPERIMENTAL PROGRAMS

2.1 Specimen fabrications

Table 1 summarizes mix proportions of concrete used in this study. The designed compressive strength of concrete at the time of the loading test was 50 N/mm^2 . The maximum size of coarse aggregates was 20 mm. Volume fraction of steel fibers was 1.0 %, that was decided by referring to Watanabe et al. (2008). The steel fiber had crimped ends, the length of 30 mm, the aspect ratio of 50, the tensile strength of $1.0 \times 10^3 \text{ N/mm}^2$, the specific gravity of 7.85, and the elastic modulus of 210 kN/mm^2 .

Figure 1 illustrates the scheme of a tested RSF beam. The specimen had the shear span (a) of 700 mm and the effective depth (d) of 250 mm; shear span to the effective depth ratio (a/d) was 2.8. The beam width (b_w) was 150 mm. In order to cause the shear failure in the specified shear span, more stirrups were provided in the opposite shear span than the test shear span. Specimens were longitudinally reinforced by two deformed PC tendons of 25.4 mm in diameter; the longitudinal reinforcement ratio (p_w) was 2.7 %. The yield strength of the PC tendon was 930 N/mm^2 as 0.2 % off-set value. These PC tendons were fixed by anchor plates and bolts to ensure sufficient anchorage. A total of three specimens with different stirrup ratio (r_w) of 0.12, 0.18, and 0.30 % were prepared. Stirrups were deformed steels of 6 mm in diameter. The yield strength was 345 N/mm^2 . The specimen was named according to volume fraction of steel fibers to full concrete (SF) and r_w ; e.g. SF10-r18 was corresponding to the specimen with $SF=1.0 \%$ and $r_w=0.18 \%$.

2.2 Loading method and measurements

RSF beams were subjected to a four-point bending

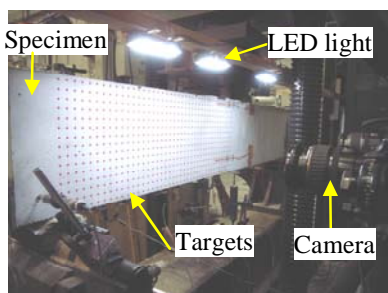


Figure 2. Loading test.

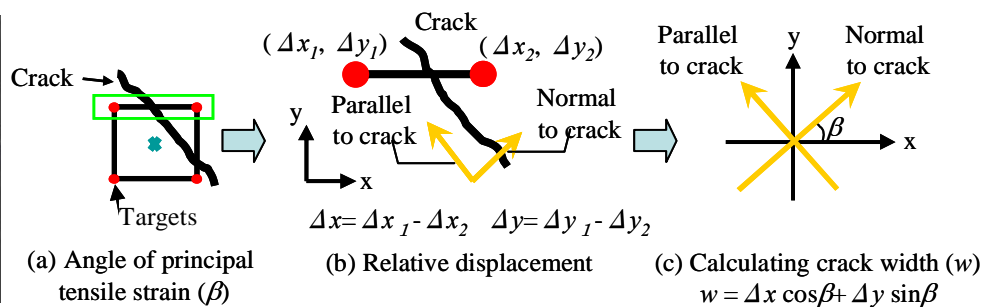


Figure 3. Calculation process of crack width by image analysis.

test. The details of loading and supporting positions are illustrated in Figure 1. Specimens were placed over roller supports, which were composed of steel plates with 50 mm width. A concentrated load was applied at the mid-span, and steel plates with 50 mm width were provided at loading points.

During the loading test, applied load, mid-span deflection, strain of the longitudinal reinforcement at the mid-span, and strain of the stirrups at the middle-height were measured by using a load-cell, transducers, and strain gauges.

2.3 Image analysis and crack width measurement

The crack width was calculated by using the displacements of targets obtained from the newly developed system. Watanabe et al. (2009) have developed the real-time image analyzing system for measuring deformation as well as strain generated on the surface of targets. The real-time image analysis requires obtaining the digital camera parameters before the start of loading by using a calibration board. The camera parameters are effective to reduce any distortion of images. Figure 2 shows the outline of loading test after the calibration. Red circular targets with diameter of 5 mm were arranged on the test span surface at an interval of 20 mm. This color is suitable for differentiating targets from the concrete surface. To improve the accuracy of image analysis, several white light-emitting diodes (LED) were put in place.

The image recorded by three digital cameras with interval of 5 kN in shear force was transferred to the computer during each loading test. Each image has 15.1×10^6 pixels (4752×3168), and is converted into HSI color space. Targets were identified by considering their characteristics: area and circularity. After computing the gravity centers of each target, the coordinates and displacements of the targets are calculated.

The crack width was defined as the displacement perpendicular to the direction of diagonal crack. Figure 3 explains the calculation process of crack width by image analysis. The angle of principal tensile strain (β) is calculated by Equation (1) at the center of the square where the crack passed. The relative displacement of two targets (Δx , Δy) located both

sides of the crack is calculated by Equation (2) (Fig. 3(b)). Then, the crack width (w) is calculated by Equation (3), and these procedures are conducted for the all set of targets on the both side of the diagonal crack (Fig. 3(c)).

$$\beta = 0.5 \tan^{-1} \left\{ \frac{\gamma_{xy}}{\varepsilon_x - \varepsilon_y} \right\} \quad (1)$$

$$\Delta x = \Delta x_1 - \Delta x_2 \quad \Delta y = \Delta y_1 - \Delta y_2 \quad (2)$$

$$w = \Delta x \cos \beta + \Delta y \sin \beta \quad (3)$$

where, ε_x is the strain of x (horizontal) direction, ε_y is the strain of y (vertical) direction, γ_{xy} is the shear strain, $(\Delta x_1, \Delta y_1)$ and $(\Delta x_2, \Delta y_2)$ are the displacement of the targets in x and y directions.

Watanabe et al. (2009) concluded that there was less than 0.05 mm in gap between the measured data through transducers and the developed system.

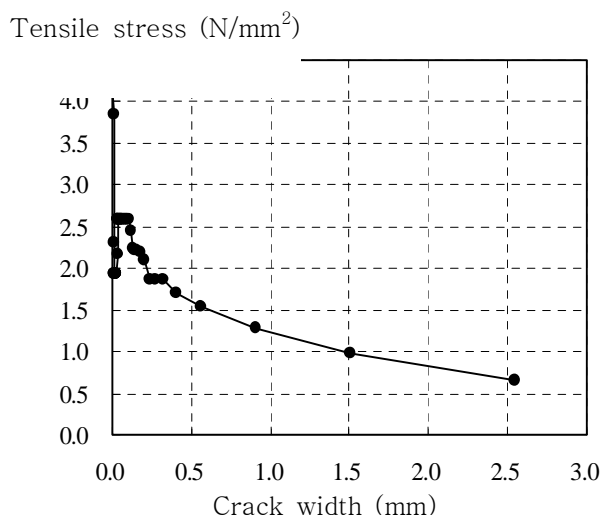


Figure 4. Tension softening curves.

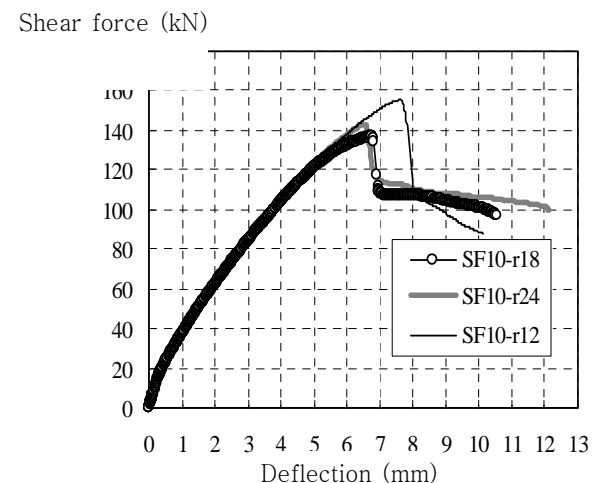


Figure 5. Comparison of shear -deflection curves.

2.4 Tension softening curves

Figure 4 indicated the tension softening curve. Five notched steel fiber reinforced concrete beams with $SF = 1.0\%$ were cast. Three point bending tests of notched beams with dimension of $100 \times 100 \times 400$ mm were conducted according to Japan Concrete Institute (JCI 2003). Tension softening curves were calculated through “tension softening curve poly-linear approximation” developed by JCI. Fracture energy (G_F) of the steel fiber reinforced concrete was 3262 N/m.

3 EXPERIMENTAL RESULTS AND DISCUSSION

3.1 Calculation of shear carried by concrete, stirrups, and fibers

The shear strength of RSF members can be calculated according to the equations presented in the JSCE design guidelines as follows (JSCE 2005, JSCE 1999):

$$V_{cal} = (1 + \kappa) \cdot V_c + V_s \quad (4)$$

$$V_c = 0.2 \cdot \sqrt[3]{f'_c} \cdot \sqrt[4]{1000/d} \cdot \sqrt[3]{100 p_w} \cdot b_w \cdot d \quad (5)$$

$$V_s = A_w \cdot f_{wy} \cdot (z/s) \quad (6)$$

where, V_{cal} : calculated value of the shear capacity for RSF member (kN), κ : coefficient ($=1.0$), V_c : shear carried by concrete (kN), V_s : shear carried by stirrups (kN), f'_c : compressive strength of concrete (N/mm^2), p_w : longitudinal reinforcement ratio ($=A_s/(b_w d)$), A_s : cross section area of longitudinal reinforcement (mm^2), A_w : cross section area of stirrups (mm^2), f_{wy} : the yield strength of stirrups (N/mm^2), z ($= (7d)/8$) (mm), and s : spacing of stirrups (mm).

An experimental value of the shear carried by steel fibers ($V_{f exp}$) was calculated by Equation (7) as follows:

$$V_{f exp} = \kappa_{exp} V_c = V_{exp} - V_c - V_s \quad (7)$$

where, V_{exp} : experimental value of the shear carrying capacity (kN), $V_{f exp}$: the shear carried by steel fibers (kN). The value of V_c and V_s were calculated through Equations (5) and (6).

A ratio of the shear carried by steel fiber to V_c is expressed by κ_{exp} as:

$$\kappa_{exp} = V_{f exp} / V_c \quad (8)$$

Table 2. Experimental results.

Specimen	Concrete properties			Diagonal crack		Shear force							
	r_w (%)	f'_c (N/mm ²)	f'_t ^{*1} (N/mm ²)	β ^{*2} (°)	Average crack width, w (mm)	Length (mm)	V_{exp} (kN)	V_c ^{*3} Eq.(5) (kN)	V_s ^{*3} Eq.(6) (kN)	V_{fexp} (kN)	V_{fcal} ^{*3} Eq.(4) (kN)	κ_{exp} Eq.(8)	V_{fcal}/V_{fex} p
SF10-r12	0.12	53.0	3.91	29	0.91	456	155.5	55.5	12.9	87.2	88.3	1.57	1.01
SF10-r18	0.18	46.6	3.45	26	0.89	473	136.8	53.2	19.3	64.4	64.6	1.21	1.00
SF10-r24	0.24	48.3	3.26	28	0.67	483	143.1	53.8	26.9	62.4	84.7	1.16	1.36

*1: tensile strength, *2: average of angle to horizontal line, *3: calculation by Eqs.(4) to (8).

3.2 Summary of experimental results

Figure 5 illustrates the shear-deflection curves of three specimens. All curves show a similar path just before the peak. This indicated that the stiffness at the beginning and the shear force when diagonal crack was generated showed similar even the value of V_{exp} were different.

Table 2 lists results of loading tests. Values of f'_c were distributed between 46.6 and 53.0 N/mm². Even r_w was increased, the value of V_{exp} was not increased when three test results were compared. All κ_{exp} : a ratio of V_{fexp} to V_c , were more than 1.0 as stated in Watanabe et al. (2008). The value of κ_{exp} became smaller with the increase in r_w . In addition, most of strain measured at stirrups in three specimens showed the yield strain in a pre-peak region.

3.3 Development of diagonal crack

Figure 6 compares the distribution of cracks taken at the peak by three cameras. All were failed in the diagonal tension failure. Even one diagonal crack was outstanding in each specimen, the diagonal crack was not observed near the top and bottom fibers.

3.3.1 Crack width increased by loading

Figure 7 plots crack width development with top horizontal axis, which was measured at the middle height of a specimen by the increase in shear force. The shear force-mid span deflection curve is also plotted in the figure with bottom axis. V_c and $V_c + V_s$ calculated by Equations (5)(6) are indicated by horizontal lines.

The diagonal crack was generated at the middle height when the shear force reached around 50kN. The shear force was not changed drastically among three specimens, and was corresponding to the value of V_c .

After the generation of diagonal crack, the crack width was increased linearly with the increase in shear force. Then, the crack width was suddenly increased when the shear force reached around 0.90 V_{max} . It was corresponding to the shear force when the shear force-mid span deflection curve also began to show non-linear near behavior the peak. Even the figure focuses on the result of crack width at the middle height of specimen, this sudden increment of diagonal crack width will be related to the peak.

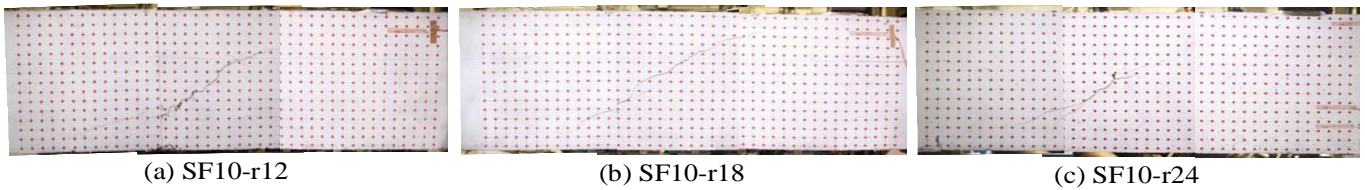


Figure 6. Crack distribution at the peak.

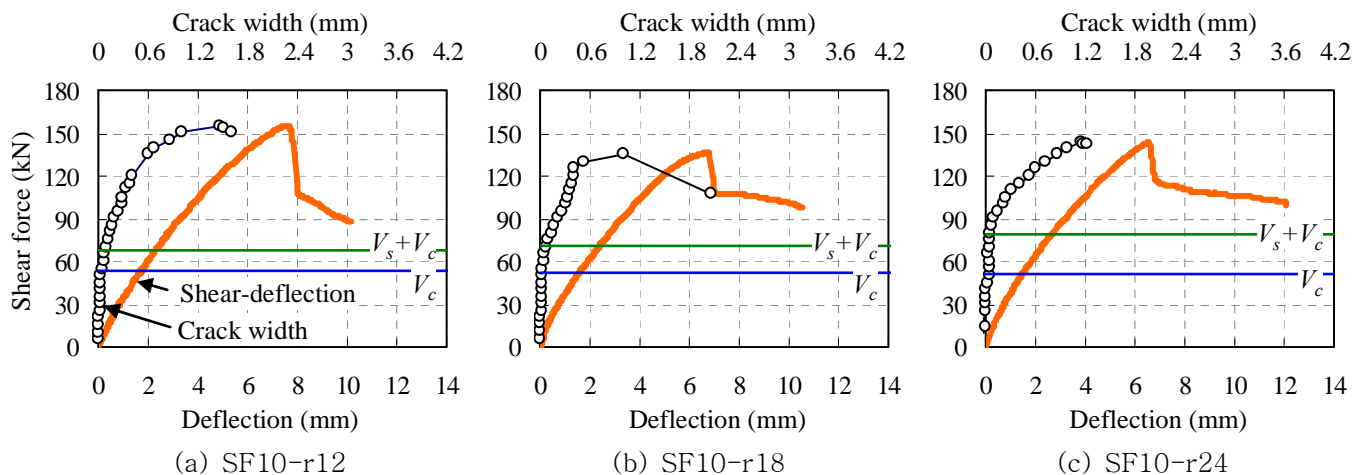


Figure 7. Development of crack width and deflection.

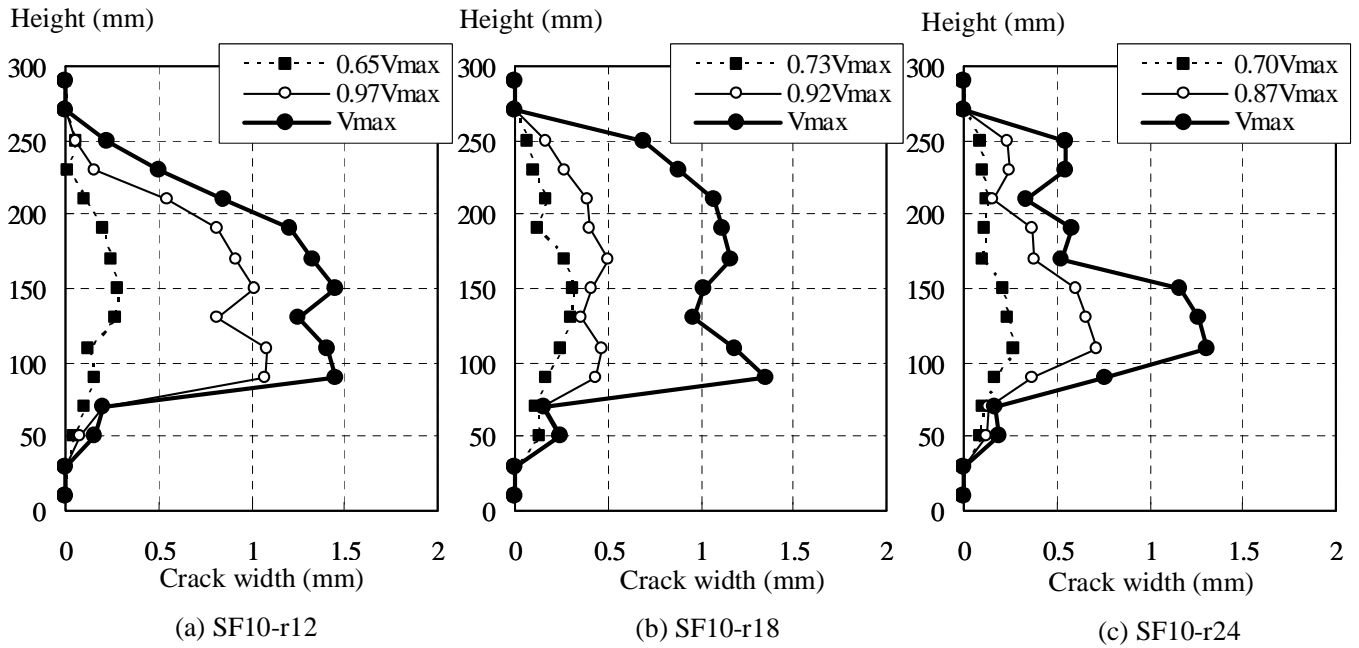


Figure 8. Distribution of diagonal crack width along the height.

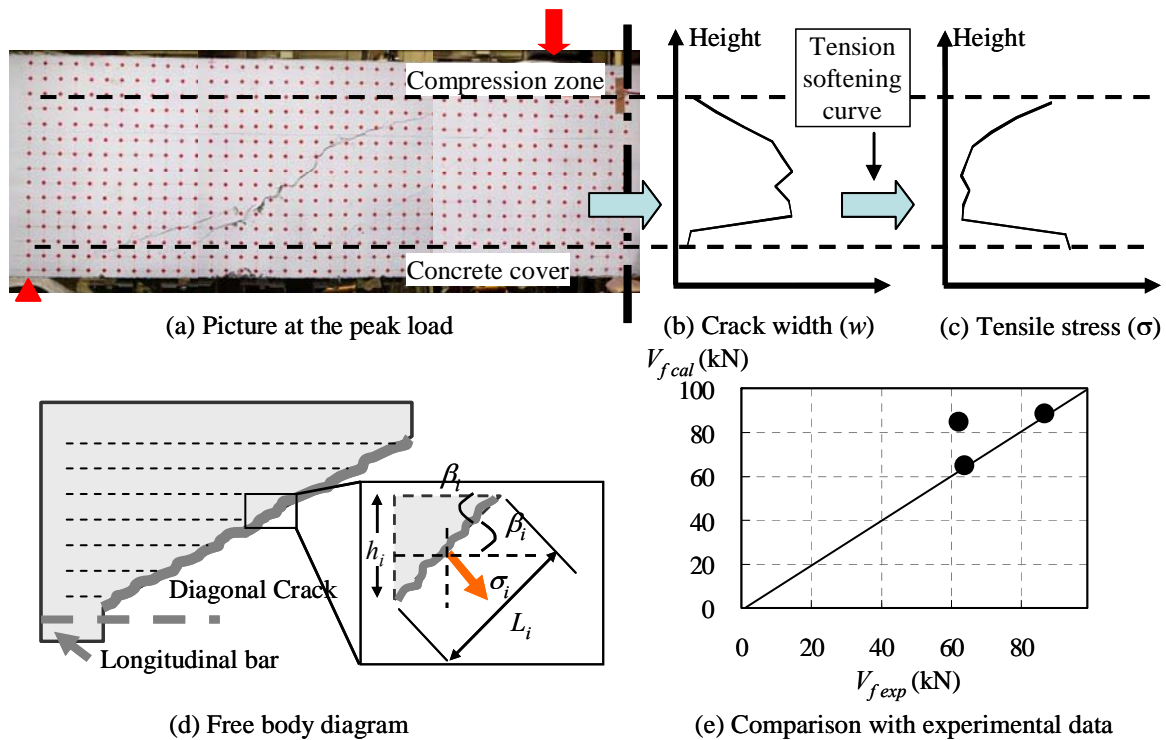


Figure 9. Calculation of shear carried by steel fibers.

3.3.2 Crack distribution along the depth

Figure 8 shows the distribution of diagonal crack width along the height of a specimen. All figures indicate that the crack width was monotonically increased with the increment of shear force at any height. The crack width became uniformly along the height at around $0.70V_{max}$. The crack width around the middle height of specimens was larger than those at the top and the bottom of specimens when the shear force was reaching V_{max} , because there was compression zone at the top flange or restriction by longitudinal bars. These three figures indicated that the average of the crack width at the peak was de-

creased with the increase in the stirrup ratio as listed in Table 2.

As mentioned in 3.3.1, the crack width was increased quickly when the shear force was reaching the peak. The image analysis has an advantage of capturing all area in one time. It seems to be difficult to measure the crack width at the peak exactly. To overcome the problem, the picture taken at the peak was compared with other pictures taken around the peak with short time interval. In addition, we confirmed that there was very slight difference between these pictures. This means the error induced by different taken-time of picture at the peak will not affect the discussion in this paper.

3.4 Shear carried by steel fibers

Figure 9 explains that the calculation of shear carried by steel fibers. The specimen was modeled as 15 layers with a height, $h_i = 20$ mm. Based on the picture taken at the peak, the values of w_i and the angle of diagonal crack, β_i , at each element were obtained through the image analysis as explained in Figure 8. By involving the tension softening curve, the crack width was converted to the tensile stress transferring across the diagonal crack, σ_i (Fig. 9(c)). Combining the crack surface area and σ_i , the force transferring across the diagonal crack by the bridging effect of steel fibers at an element can be obtained.

Conventionally, some contributions have been reported as a shear resistance mechanism such as the resistance in compression zone, interlocking by aggregates, the dowel action by longitudinal bars, and tensile force by stirrups, and expressed as $V_c + V_s$ in the modified truss analogy (MacGregor & Wight 2004).

Figure 9(d) shows the free body diagram of a RSF beam, which focuses on the contribution by steel fibers. According to the result of Figure 8, the force was generated along the diagonal crack except for the compression zone and concrete cover. Vertical component of this force with the consideration of β_i would be corresponding to the shear carried by steel fiber. Finally, the value of V_{fcal} was calculated by the equation as follows:

$$V_{fcal} = \sum (\sigma_i \cdot b_w \cdot L_i \cdot \cos \beta_i) = \sum \frac{\sigma_i \cdot b_w \cdot h_i}{\tan \beta_i} \quad (9)$$

The calculated values of V_{fcal} by Equation (9) and V_{fexp} by Equation (7) were compared in Figure 9 (e) and listed in Table 2.

V_{fcal} in SF10-r24 was larger than V_{fexp} . This was caused by relatively smaller crack width between height of 165 and 195 mm. If the crack width increases, the V_{fcal} will be closer to the V_{fexp} . There was a potential to induce a synergetic effect on V_c by fiber: e.g. interlocking by aggregates. On the other hand, V_{fcal} in SF10-r12 and SF10-r18 showed good agreement with V_{fcal} . This V_{fcal} will be used for predicting the shear carried by steel fiber. The increase in number of the specimen is required; however, these findings imply that the shear carried by steel fiber can be evaluated by using the tension softening curve.

4 CONCLUSIONS

(1) A ratio of the shear carried by steel fiber to the shear carried by concrete, V_{fcal}/V_{fexp} , was changed depending on stirrup ratio, r_w .

(2) The crack width at the middle height of some specimens was suddenly increased when the shear

force reached around 90 % of the shear strength of RSF beams, V_{max} .

(3) The crack width around the middle height of specimens was larger than those at the top and the bottom surfaces of a specimen.

(4) The shear carried by steel fiber calculated by using the tension softening curve corresponded to the experimental value.

(5) The shear carrying mechanism and shear carried by steel fiber of RSF beams can be evaluated by using the tension softening curve.

This work was partially supported by the Grant-in-Aid for Scientific Research (A) (No.19206050) from Japan Society for Promotion of Science.

REFERENCES

- Japan Concrete Institute (JCI). 2003. Method of test for load-displacement curve of fiber reinforced concrete by use of notched beam.
- Japan Society of Civil Engineers (JSCE). 1999. Guidelines of Design for RSF Piers. Concrete Library 97. (in Japanese)
- Japan Society of Civil Engineers (JSCE). 2005. Standard Specifications for Concrete Structures-2002, Structural Performance Verification.
- MacGregor, J. G. & Wight, J. K. 2004. Reinforced Concrete Mechanics and Design, Prentice Hall.
- Watanabe, K. Kimura, T. and Niwa, J. 2008. Shear reinforcement of RC beams by combination of steel fibers and stirrups. Proc. of the 3rd ACF International Conference-ACF/VCA. 790-765.
- Watanabe, K. Higashi, H. & Niwa, J. 2009. Real-time image analyzing system for evaluating the shear failure mechanism of reinforced concrete beams. 4th International Conference on Construction Materials: Performance, Innovations and Structural Implications (ConMat'09). 1477-1482.